*Human Molecular Genetics, 2007, Vol. 16, No. 2* ***173–186***
*doi:10.1093/hmg/ddl459*
*Advance Access published on December 21, 2006*

# The Meckel–Gruber Syndrome proteins MKS1 and meckelin interact and are required for primary cilium formation

**Helen R. Dawe[1,†], Ursula M. Smith[2,†], Andrew R. Cullinane[2], Dianne Gerrelli[4], Phillip Cox[5], Jose L. Badano[6], Sarah Blair-Reid[2,3], Nisha Sriram[1], Nicholas Katsanis[6], Tania Attie-Bitach[7], Simon C. Afford[3], Andrew J. Copp[4], Deirdre A. Kelly[8], Keith Gull[1] and Colin A. Johnson[2,*]**

[1]Sir William Dunn School of Pathology, University of Oxford, South Parks Road, Oxford OX1 3RE, UK, [2]Section of Medical and Molecular Genetics, Division of Reproductive and Child Health and [3]The Liver Research Laboratories, Institute of Biomedical Research, University of Birmingham Medical School, Vincent Drive, Edgbaston, Birmingham B15 2TT, UK, [4]Neural Development Unit, Institute of Child Health, University College London, 30 Guilford Street, London WC1N 1EH, UK, [5]Department of Histopathology, Birmingham Women's Hospital, Metchley Park Road, Birmingham B15 2TG, UK, [6]McKusick Nathans Institute of Genetic Medicine, Johns Hopkins University School of Medicine, 733 N. Broadway, Baltimore, MD 21205, USA, [7]Département de Génétique et INSERM U-393, Hôpital Necker Enfants-Malades, 149 rue de Sèvres, Paris 75743, France and [8]Children's Liver Unit, Princess of Wales Children's Hospital, Steelhouse Lane, Birmingham B4 6NH, UK

Received September 21, 2006; Revised and Accepted December 5, 2006

**Meckel–Gruber syndrome (MKS) is an autosomal recessive lethal malformation syndrome characterized by renal cystic dysplasia, central nervous system malformations (typically, posterior occipital encephalocele), and hepatic developmental defects. Two MKS genes, *MKS1* and *MKS3*, have been identified recently. The present study describes the cellular, sub-cellular and functional characterization of the novel proteins, MKS1 and meckelin, encoded by these genes. *In situ* hybridization studies for *MKS3* in early human embryos showed transcript localizations in agreement with the tissue phenotype of MKS patients. Both MKS proteins predominantly localized to epithelial cells, including proximal renal tubules and biliary epithelial cells. MKS1 localized to basal bodies, while meckelin localized both to the primary cilium and to the plasma membrane in ciliated cell-lines and primary cells. Meckelin protein with the Q376P missense mutation was unable to localize at the cell membrane. siRNA-mediated reduction of *Mks1* and *Mks3* expression in a ciliated epithelial cell-line blocked centriole migration to the apical membrane and consequent formation of the primary cilium. Co-immunoprecipitation experiments show that wild-type meckelin and MKS1 interact and, in three-dimensional tissue culture assays, epithelial branching morphogenesis was severely impaired. These results suggest that MKS proteins mediate a fundamental developmental stage of ciliary formation and epithelial morphogenesis.**

## INTRODUCTION

Johann Friedrich Meckel described the clinical entity that subsequently became known as Meckel syndrome in 1822 (1) in two newborn children presenting with occipital encephalocele, polydactyly, cleft palate and large cystic kidneys. The condition was called dysencephalia splanchnocystica by Gruber (2), John Marius Opitz further delineated the syndrome (3) and it has since been referred to as Meckel–Gruber syndrome (MKS). The classic triad of features associated with MKS are cystic kidneys (100% of cases), occipital encephalocele (90%) and polydactyly (<80%) (4,5). However, the

*To whom correspondence should be addressed. Fax: +44 1216272618; Email: c.a.johnson@bham.ac.uk;
†The authors wish it to be known that, the first two authors should be regarded as joint First Authors.

clinical phenotype has been extended and altered since the disorder was first characterized and there is known to be a wide phenotypic variation. It has been suggested that at least two of the classic manifestations should be present to establish a definitive MKS diagnosis (6) or one classic feature and two other relevant anomalies (7). Central nervous system (CNS) abnormalities associated with MKS include Dandy-Walker malformation, agenesis of the corpus callosum, microcephaly, rhombic roof dysgenesis and prosencephalic dysgenesis. It has been suggested that a distinctive triad of CNS malformations (prosencephalic dysgenesis, occipital encephalocele and rhombic roof dysgenesis) should be included in the diagnostic criteria of MKS (8). Fibrocystic changes to the liver are possibly the only other constant finding, typically manifesting as impeded development of the intrahepatic biliary system and ductal plate malformation (4,7). Other associated MKS features include post-axial polydactyly, cleft lip/palate, laterality defects and congenital heart malformations including dextrocardia, shortening and bowing of the long tubular bones and abnormal development of the male genitalia. Survival beyond birth is unusual with a majority of cases dying *in utero*. Incidence is variable and high frequencies have been estimated in North Africa (1:3500) and Finland (1:9000) (5). In the USA, the incidence is reported to be 1:13 250 (9).

MKS displays locus heterogeneity and, to date, three loci have been identified. *MKS1* was mapped to chromosome 17q21-q24 in an endogamous Finnish population (10) and, more recently, Kyttälä *et al*. (11) redefined the critical *MKS1* locus to a region $<100$ kb through linkage disequilibrium and identified mutations in the novel gene *FLJ20345/MKS1*. *MKS1* encodes a protein, MKS1, of previously unknown function. MKS1 is 559 amino acids in length, lacks any predicted transmembrane helices but contains a B9 domain, the significance of which is currently unknown. Broad tissue expression of this gene was reported, although increased expression was identified in the brain, liver, kidney and the cartilage tissue of the developing digits of the upper limbs. *MKS1* has been previously identified as a gene within the flagella and basal body proteome (FABB; see the ciliary proteome web server http://www.ciliaproteome.org/ (12), suggesting a link between MKS and ciliary or basal body function that is borne out by the clinical features (13).

Roume *et al*. (14) reported locus heterogeneity in eight families of North African and Middle Eastern ancestry. Subsequent autozygosity mapping in seven consanguineous families revealed a second MKS locus, *MKS2*, on chromosome 11q13 (15). The region spans $\sim$8 cM and a causative gene is yet to be identified.

*MKS3* was mapped to chromosome 8q24 (16) and, recently, we reported the identification of mutations in the novel gene, *MKS3/TMEM67*, in a cohort of six MKS cases originating from Pakistan and Oman (17). In addition, a missense mutation was identified in the rat orthologue, *LOC313067/Tmem67*, in the wpk rat model of MKS, which is characterized by polycystic kidney disease and CNS malformations, including hypoplasia to agenesis of the corpus callosum and severe hydrocephalus (18). At the RNA level, we found ubiquitous, moderate expression of *MKS3*, with higher expression in embryonic adrenal gland, brain, kidney, lung and spinal cord. The predicted protein, meckelin, comprises 995 amino acids in humans, and although it is evolutionarily conserved with orthologues, for example, in *Caenorhabditis elegans* and *Drosophila melanogaster*, it has no known paralogues. The predicted structure of meckelin has some topological similarity with the Frizzled (FZD) family of receptor proteins, which are thought to have diverse roles in signal transduction during differentiation and development by the Wnt class of ligands [reviewed in (19)]. A role for *FZD4* in retinal angiogenesis has been suggested by the identification of mutations in a subset of patients with familial exudative vitreoretinopathy (EVR) (20). Frizzled receptors also have a role in establishing and maintaining epithelial planar cell polarity (PCP) during morphogenesis in both *D. melanogaster* and vertebrates [reviewed in (21)]. In addition, the *MKS3* promoter sequence contains an X-box motif, a sequence known to be involved in the regulation of primary ciliary genes in *C. elegans* (22), and therefore clearly implicates meckelin in mediating primary ciliary function.

Here, we provide the first evidence of the localization and function of the novel proteins MKS1 and meckelin. To determine the cellular and sub-cellular localization of the novel proteins, MKS1 and meckelin, we raised specific polyclonal antibodies for use in a series of western blotting, immunohistochemical staining and immunofluorescence microscopy studies. Furthermore, we used siRNA-mediated reduction of *Mks1* and *Mks3* expression in a ciliated cell-line to characterize the roles of these proteins in ciliogenesis.

## RESULTS

### *In situ* hybridization studies of *MKS3*

The expression of *MKS3* mRNA was determined by a series of *in situ* hybridization experiments on human embryo sections (Fig. 1). A sense RNA control probe, transcribed from nucleotides 2289 to 3070, which contains much of the 3′-UTR of *MKS3*, gave a negligible background signal (Fig. 1A and C; data not shown). An antisense probe for *SHH* was used as a positive control for staining, with specific and restricted expression in the gut, notochord and floor plate of the CNS (data not shown). In the embryonic brain, an antisense probe for *MKS3* revealed moderate to high levels of expression restricted to ventral midline regions of the posterior forebrain (Fig. 1B), particularly the hindbrain floor (Fig. 1E) and the developing sphenoid bone (Fig. 1F). *MKS3* was also expressed at moderate levels in post-mitotic neurons in the midbrain and posterior forebrain (Fig. 1E). Intense expression of *MKS3* was detected in the cartilage of developing limbs, particularly in the digits (Fig. 1J'), the cartilaginous cervical vertebrae (Fig. 1D, E, H, I and J), the bronchioles of the lung (Fig. 1H), intestine (Fig. 1D and I), stomach (Fig. 1D, G and I) and kidney (Fig. 1D, G and I). Expression was also noted in large intrahepatic bile ducts (Fig. 1G and I) and in the outer layer of the developing retina (Fig. 1K and K').

### Immunohistochemical detection of meckelin and MKS1

To determine the cellular and sub-cellular localization of meckelin and MKS1, we developed polyclonal antisera against synthetic peptides. The specificities of the antisera were characterized by ELISA assays (data not shown) and

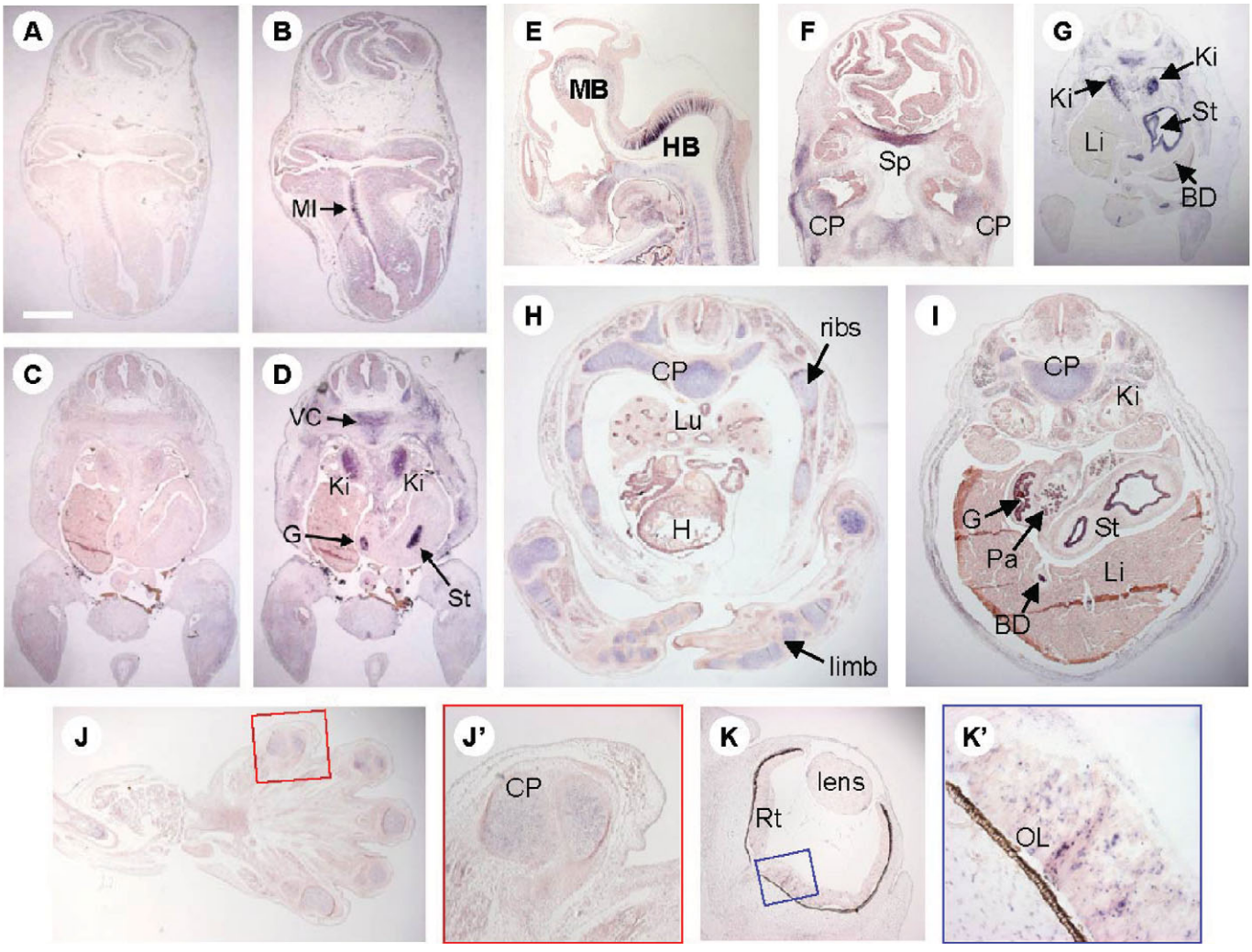


**Figure 1.** *In situ* hybridization of *MKS3* transcript distribution in human embryos. (**A**) Negative control hybridization with sense RNA and (**B**) antisense RNA probe of brain frontal section through embryo at Carnegie stage (CS) 16 (gestation age 37–42 days). MKS3 transcripts are particularly abundant in the ventral midline of the posterior forebrain. (**C**) Sense and (**D**) antisense RNA probes for transverse sections of CS16 embryo; intense *MKS3* expression is seen in developing vertebral cartilage, kidney, intestine and stomach. (**E**) Sagittal section of a CS16 embryo showing strong hindbrain floor staining, in addition to expression in post-mitotic neurons in the midbrain and posterior forebrain region. (**F**, **G**) Transverse sections of a CS16 embryo showing *MKS3* expression in cartilage primordia, kidney, stomach and large intrahepatic bile ducts of the liver. Note the particularly intense expression in the developing sphenoid bone. (**H**, **I**) Transverse sections of CS22 embryos (gestational age 54–56 days) with intense expression in cartilage primordia including those of ribs and upper limbs, as well as in lung, heart and pancreas. (**J**) Transverse section of the embryonic hand at CS23 (gestational age 56–60 days). The enlargement (**J'**) shows expression in the cartilage primordium of a digit. (**K**) Section through the eye in a CS20 (gestational age 51–53 days) embryo, with the enlargement (**K'**) showing expression in the outer layer of the retina. BD, large intrahepatic bile ducts; CP, cartilage primordia; G, intestine; H, heart; HB, hindbrain; Ki, kidney; Li, liver; Lu, lung; MB, midbrain; Ml, midline of posterior forebrain; OL, outer layer of retina; Pa, pancreas; Rt, retina; Sp, sphenoid bone; St, stomach; VC, vertebral cartilage. Bar: (A–G) 100 μm; (H and I) 38 μm; (J) 154 μm; (J' and K) 476 μm; (K') 2380 μm.

western blotting, which showed that they detected single bands of expected size 70 kDa (for anti-MKS1) and 120 kDa (for meckelin) (Fig. 2A). We also determined the absolute levels of expression of the *Mks1* and *Mks3* genes using quantitative real-time PCR with *Hprt* as a normalizing control. *Mks1* and *Mks3* were expressed at 41 and 46% of the level of *Hprt*, respectively. Hprt is between 0.01 and 0.1% of total cellular protein (23).

We visualized the location of meckelin and MKS1 in sections from fixed, paraffin-embedded liver and kidney tissue blocks (Fig. 2B and C) obtained between weeks 18 and 20, at the time of termination of pregnancy, for two gestationally age-matched normal controls (Fig. 2B) and three MKS cases (Fig. 2C). Two of the MKS cases had *MKS3* mutations that have been reported previously (17); the remaining case had a novel *MKS1* frameshift mutation. In normal controls and in agreement with our *in situ* hybridization experiments for *MKS3* (Fig. 1) and those reported previously for *MKS1* (11), moderate to high levels of meckelin and MKS1 were localized at the proximal renal tubule epithelia, but not at the glomeruli (Fig. 2B), and at the biliary epithelium of larger bile ducts (data not shown). Diffuse background staining of hepatocytes was also detected, but since this was also present in pre-immune negative controls we ascribe this to endogenous

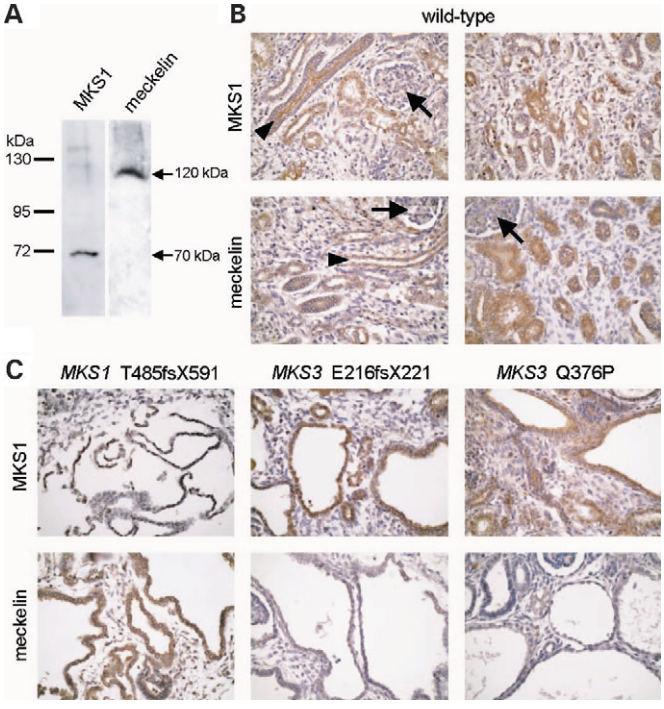


**Figure 2.** Western blotting and immunohistochemical staining with anti-MKS1 and anti-meckelin antisera. (**A**) Immunodetection of MKS1 (70 kDa) and meckelin (120 kDa) in WCEs of HEK293 cells; molecular weight size standards are indicated on the left. (**B**) Immunohistochemical staining of normal control fetal week 18–20 kidney tissue sections with anti-MKS1 and anti-meckelin antisera. Note the intense staining in proximal renal tubules (arrowheads) but not in the glomeruli (arrows). (**C**) Immunohistochemical staining of kidney tissue from MKS cases with the frameshift mutations *MKS1* 1448_1451dupCAGG (T485fsX591) (left panels) and *MKS3* E216fsX221 (middle panels), and the *MKS3* Q376P missense mutation (right panels). Original magnification (B and C), 400 × .

peroxidase activity. For MKS cases, MKS1 was not detected in the epithelial cell layer of the renal cysts for case 102, which had a homozygous *MKS1* c.1448_1451dupCAGG duplication causing a frameshift mutation (p.T485fsX591) and is therefore a null allele. Complete loss of meckelin expression was also seen for case 67F, with a homozygous frameshift mutation c.647delA (p.E216fsX221), for which we have already confirmed the complete absence of *MKS3* transcript in fetal liver tissue (17). Meckelin immunostaining was also absent for case 40T with a homozygous missense mutation c.1127A>C (p.Q376P), but we ascribe this to the accumulation of the mutant protein in the endoplasmic reticulum (ER) (see below). Expression of protein from the wild-type *MKS* gene was not affected in any of the three cases, with strong staining in the epithelial cell layer of renal cysts (Fig. 2C).

### Aberrant localization of mutant meckelin with missense mutation Q376P

As *MKS3* encodes meckelin, a putative transmembrane receptor (17), we assessed the localization of HA-tagged wild-type meckelin and an HA-tagged mutant protein with the Q376P missense change in RCC4 and HEK293 cells, which are derived from proximal renal tubular epithelium and are therefore likely to process nascent proteins in a physiologically relevant fashion. Cell surface localization was apparent in permeabilized RCC4 cells that expressed wild-type meckelin, but not cells that expressed the Q376P mutant (Fig. 3A). We quantified the number of HEK293 cells transfected with either wild-type meckelin ($n = 194$) or meckelin Q376P ($n = 154$), and also the number of transfected cells with either clear cell surface localization of HA-tagged protein, or only intracellular localization (Fig. 3C). Protein with the missense mutation displayed statistically significant intracellular accumulation (unpaired $t$ test; $P < 0.001$) that predominantly co-localized with anti-calreticulin antibody (Fig. 3D, arrows), suggesting retention in the ER. We also determined some co-localization with EEA1, a marker of early endosomes (data not shown). Thus, cell-surface accumulation of the wild-type protein is consistent with its functional role as a transmembrane receptor, with a possible role for the extracellular domain of meckelin in mediating intracellular transport from the ER.

We labelled transfected cells with the membrane-impermeant biotin compound sulfo-NHS-SS-biotin to analyse cell surface processing of meckelin. While both HA-tagged wild-type meckelin protein and the Q376P mutant protein were expressed at high levels (Fig. 3E), pull-down of biotinylated proteins with streptavidin-agarose demonstrated that only wild-type meckelin was biotinylated and therefore found at the cell surface (Fig. 3E).

### Meckelin localizes to primary cilia and MKS1 to centrosomes

We investigated the sub-cellular localization of endogenous MKS1 and meckelin in HEK293 cells and biliary epithelial cells (BECs). As expected, meckelin had a widespread distribution at the border of HEK293 cells (Fig. 4A, arrowheads), and very high expression in BECs (data not shown, and Fig. 4B), with co-localization at primary cilia indicated by intense staining with anti-acetylated α-tubulin (Fig. 4A and B, white arrows). In contrast, MKS1, a putative cytoplasmic protein (11), had a broad intracellular localization with occasional distribution at the border of HEK293 cells (white arrowhead in Fig. 4A), but was absent from primary cilia (marked by white arrows) in both HEK293 cells and BECs. However, MKS1 clearly displayed a punctuate doublet staining pattern characteristic of a centrosomal localization in BECs (green arrows in Fig. 4B). To confirm this, we transiently transfected a number of cell-lines, including IMCD-3 cells, which are derived from mouse inner medullary collecting duct, and HEK293 cells, with Myc-tagged MKS1 and showed co-localization with anti-γ-tubulin (Fig. 4C, white arrows), a marker of centrosomes and basal bodies (in post-mitotic cells).

### MKS1 and meckelin are required for ciliogenesis

We tested the effect of silencing *Mks1* or *Mks3* on ciliogenesis. We used a pool of three to four siRNA duplexes targeted against either *Mks1* or *Mks3*. Each pool was transiently transfected into IMCD-3 cells, and the presence of cilia assessed 96 h later using anti-acetylated α-tubulin antibody as a ciliary marker. We used quantitative real-time PCR assays

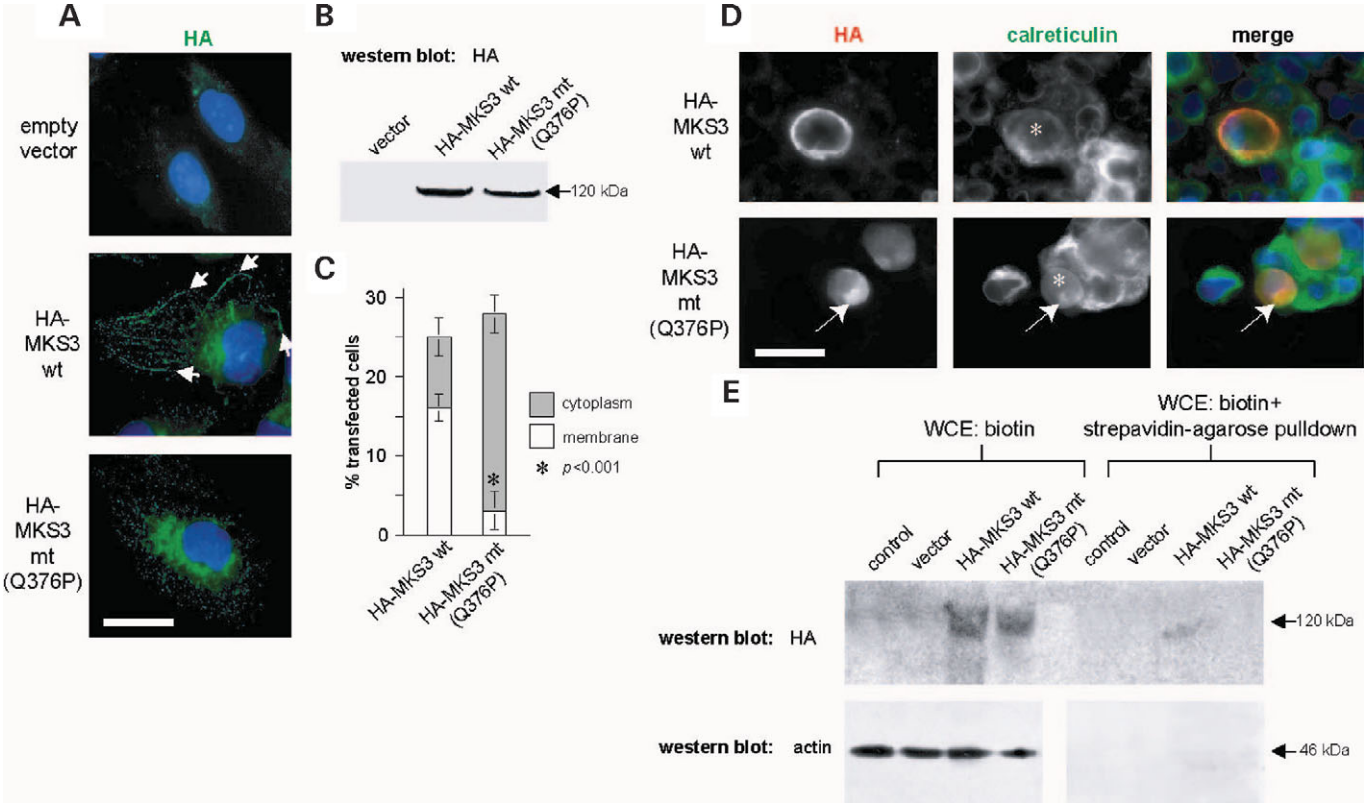


**Figure 3.** Functional characterization of the meckelin Q376P missense mutation. (**A**) Immunofluorescence microscopy of transiently transfected RCC4 cells, showing localization of wild-type HA epitope-tagged meckelin (HA-MKS3 wt; middle panel) at the cell surface (arrows), but not mutant meckelin [HA-MKS3 mt(Q376P); bottom panel]. Bar: 5 μm. (**B**) Immunodetection of equal levels of wild-type and mutant HA-tagged meckelin in WCEs of transiently transfected cells, with transfection of empty vector (first lane) as the negative control. (**C**) Quantification of the sub-cellular localization of wild-type and mutant HA-tagged meckelin at either the cell surface ('membrane', white bars) or at all other intracellular locations in the cells (but predominantly the ER) excluding the cell surface ('cytoplasm', grey bars). An unpaired *t*-test for cells transfected with wild-type ($n = 194$) and mutant ($n = 154$) meckelin showed a statistically significant difference in cell surface localization ($^*P < 0.001$). (**D**) Immunofluorescence microscopy of HEK293 cells transiently transfected with either wild-type HA-MKS3 wt (top panel) or mutant HA-MKS3 mt(Q376P) (bottom panel) (images on the left), with visualization of the ER using anti-calreticulin (centre images). Transfected cells are indicated by an asterisk. Full colour merged images are shown on the right. Arrows show co-localization at the ER. Bar: 10 μm. (**E**) Analysis of cell surface processing of epitope-tagged wild-type and mutant HA-meckelin, following transient transfection of HEK293 cells; both wild-type and mutant meckelin were expressed at equal levels by western blotting of total input WCE ('WCE: biotin'; top left panel) with an anti-HA antibody. Biotinylated cell-surface proteins pulled-down by streptavidin-agarose ('WCE: biotin+ streptavidin-agarose pulldown'; top right panel) include only wild-type meckelin. Western blotting for β-actin (bottom panels) controlled for loading (left) and non-biotinylation of intracellular proteins (right).

to determine that RNAi had been successful, with total transcript levels for *Mks1* at 15 ± 2.3% that of negative controls, and *Mks3* at 33.7 ± 2%. In contrast to wild-type (data not shown) and negative control siRNA-transfected (Fig. 5A) cells, ciliary formation was markedly reduced in *Mks1*- (Fig. 5B) and *Mks3*- (Fig. 5C) silenced cells, although centrioles/basal bodies could still be observed with anti-γ-tubulin antibody. Sixty-five percentage of negative control-transfected cells showed ciliary staining, while *Mks1*- and *Mks3*-silenced cells displayed only 18 and 25% ciliary staining, respectively (Fig. 5D). Silencing of the intraflagellar transport protein IFT-88 (24) was used as a positive control for loss of cilia; <10% of *IFT-88*-silenced cells exhibited ciliary staining. Cilia in *Mks1*- and *Mks3*-silenced cells, when present, were significantly shorter than control cells (Student's *t*-test, $P < 0.001$), with an average length of 2.5 ± 0.16 μm for *Mks1*-silenced cells and 4.3 ± 0.20 μm for *Mks3*-silenced cells when compared with 7.4 ± 0.27 μm for negative control-transfected cells. Simultaneous silencing of *Mks1* and *Mks3* yielded the same phenotype as the individual silencing experiments.

We asked whether this effect on cilium formation could be caused by a general perturbation of apical–basal polarity. The establishment of cell–cell contacts is essential for epithelial polarity and tissue morphogenesis (25,26). We tested the effect of *Mks1*- or *Mks3*-silencing on the subcellular localization and distribution of the tight-junction marker ZO-1 and the adherens junction marker E-cadherin and found no difference in the localization or appearance of either marker compared with negative control-transfected cells (data not shown). We measured the transepithelial resistance across the monolayer of *Mks1*-, *Mks3*- and negative control-silenced cells. No significant differences were observed after 5 days of culture on Transwells (data not shown). Finally, we assessed whether *Mks1*- and *Mks3*-silenced cells retained the ability to differentiate their apical membrane and form microvilli. Scanning electron microscopy revealed the expected loss of cilia (Fig. 5E–G. However, *Mks1* or *Mks3* siRNA-transfected

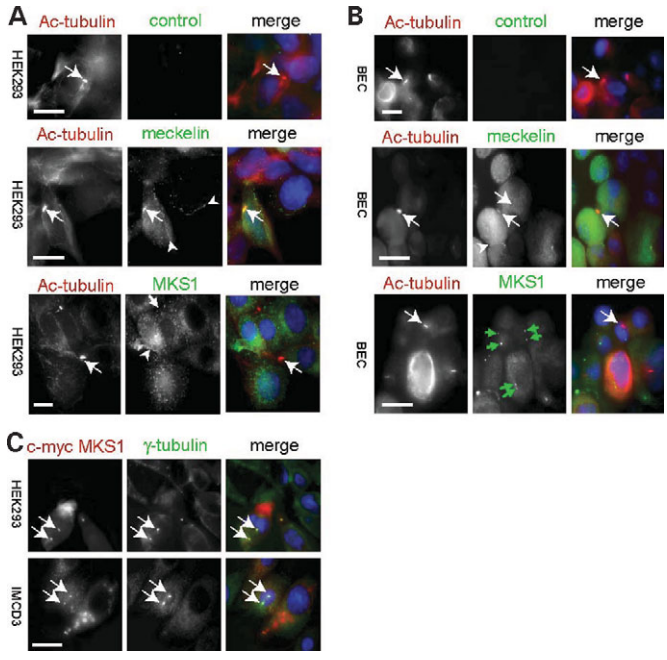


**Figure 4.** Immunofluoresence microscopy with anti-meckelin and anti-MKS1 antisera. Labelling of (**A**) confluent, post-mitotic HEK293 cells and (**B**) polarized, primary cells (BECs) with pre-immune serum (top), anti-meckelin (middle) and anti-MKS1 (bottom). Primary cilia (white arrows) are visualized using anti-acetylated α-tubulin. Full colour merged images including the cell nuclei (visualized with DAPI) are shown on the right. Note the localization of meckelin, but not MKS1, to the primary cilium in both HEK293 cells and BECs (white arrows). Note also the punctuate doublet staining suggestive of centrosomes observed with anti-MKS1 in BEC cells (green arrows). Cell surface localization of meckelin and MKS1 are indicated by arrowheads. Bar: 5 μm. (**C**) Co-localization of myc epitope-tagged MKS1 (left) with γ-tubulin (centre), a specific marker of the centrosome/basal body, in HEK293 and IMCD3 cells. Bar: 5 μm.

cells additionally had fewer microvilli (Fig. 5E'–G'). We quantified the number of microvilli present in a 25 $\mu m^2$ region at the centre of each cell and found significant differences between negative control-transfected cells and *Mks1*- or *Mks3*-silenced cells (Student's *t*-test result: $P < 0.001$ compared with control cells for *Mks1*-silenced cells and $P < 0.005$ compared with control cells for *Mks3*-silenced cells). An average of $71 \pm 3.8$ microvilli were present within the defined region in the negative control-transfected cells, while *Mks1*- and *Mks3*-silenced cells had an average of $39 \pm 2.6$ and $45 \pm 3.1$ microvilli, respectively, suggesting a possible polarization defect independent of the ability to form functional junctions.

All cilia are extended from a basal body (27,28). The primary cilium is extended from a single basal body analogous to the pre-existing mature centriole in the cell. In dividing IMCD-3 cells, the centrosome (two centrioles surrounded by a pericentriolar matrix) is localized in a juxtanuclear position closely associated with the nuclear envelope (data not shown). To form a primary cilium, the centrioles must migrate to and dock with the apical membrane by an as yet unknown mechanism. We therefore asked whether the inability to form a cilium was due to incorrect positioning of the centriole/basal body. Anti-γ-tubulin was used to mark the position of the centrosome. Z-stacks were taken every 0.5 μm and cells were scored according to whether the γ-tubulin labelling was observed in an apical position (within the first 2.5 μm of the cell, above the nucleus), in the mid-cell region or in the basal region of the cell (below the nucleus, in the last 1 μm of the cell). γ-Tubulin staining was present in the apical region of the cell in 58% of negative control-transfected cells (Fig. 6A, arrow); however, the number of cells with an apically positioned centrosome was reduced to 28 and 24% in *Mks1*- and *Mks3*-silenced cells, respectively (Fig. 6C). Instead, the γ-tubulin label was positioned in the mid-cell region (Fig. 6B, arrow). As a control experiment, we assessed centrosome positioning in IFT-88-silenced cells as these do not form cilia (see above), but centriole migration should not be impaired. γ-Tubulin staining was apparent in the apical region of the cell in 63% of *IFT-88*-silenced cells, indicating that intraflagellar transport is not required for centriole migration.

## MKS1 and meckelin are required for cell branching morphogenesis

Under normal circumstances, sheets of epithelial cells within the kidney form an elaborate network of tubules. Given that one of the classic clinical manifestations of MKS is the formation of large cystic kidneys suggestive of a gross impairment of tubulogenesis, we asked whether silencing of *MKS1* or *MKS3* affected branching morphogenesis and tubulogenesis. Unlike other epithelial cell lines such as MDCK, IMCD-3 cells spontaneously form highly branched structures and tubules in three-dimensional culture (29,30). Branched structures are formed within 72 h of three-dimensional culture (Fig. 7A). Tubules are just beginning to form at this stage, although apical–basal polarity is not yet fully determined (Fig. 7B); they can be clearly seen after 10 days of collagen culture (data not shown). To test whether silencing *MKS1* or meckelin would induce abnormal branching morphology, we transfected cell monolayers with the pooled siRNAs and 24 h later placed the cells into a three-dimensional collagen I matrix culture. Cultures transfected with either siRNA pool showed a decrease in the number of elongated and branched structures visible within the gel compared with the negative control-transfected cultures. Instead, cells aggregated into clumps with few small branches (Fig. 7C and D). At the ultrastructural level, clusters of cells were visible adjacent to hollow cysts (Fig. 7E, arrow marks the cyst). Elongated branched structures failed to form in 75–80% of *MKS1*- or *MKS3*-silenced cell colonies (Fig. 7F) as opposed to around one-third of negative control-transfected cell colonies. This significant decrease in the frequency of branched structures ($\chi^2$ test: $P < 0.001$, $n = 150–300$ cell colonies) suggests that reduction of MKS1 or meckelin expression prevents tubule formation by perturbing early branching morphogenesis in three-dimensional cultures.

## Meckelin and MKS1 interact

The similar siRNA phenotypes observed for MKS1 and meckelin suggest that they may act in a common pathway. We determined that endogenous meckelin had a widespread

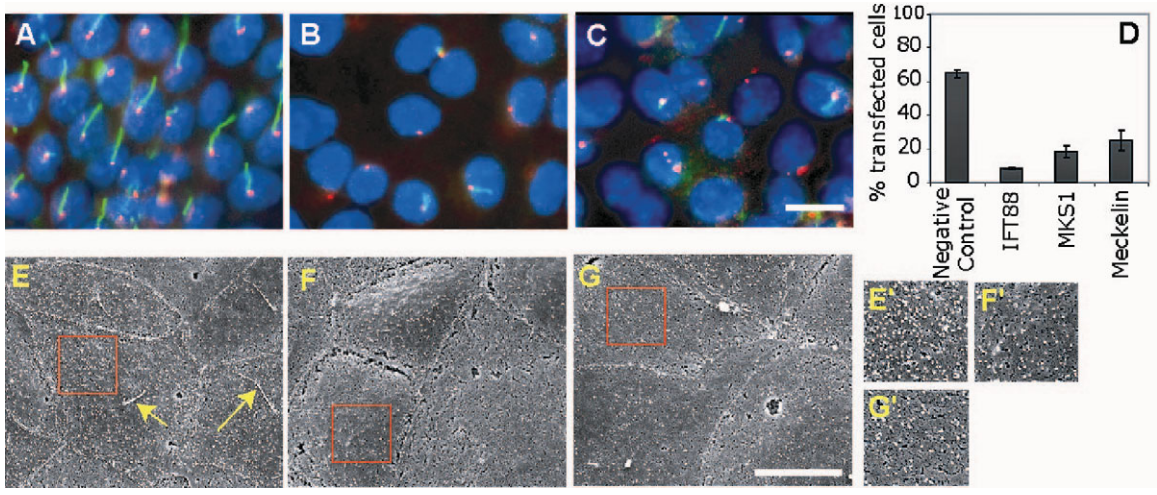


**Figure 5.** MKS1 and meckelin are required for ciliogenesis. Immunofluorescence (**A–C**) and scanning electron microscopy (**E–G**) of IMCD-3 monolayers transfected with negative control siRNA (A and E), siRNA against *MKS1* (B and F) or siRNA against *MKS3* (C and G). (A–C) Note the loss of primary cilia (acetylated α-tubulin staining, green) in *MKS1*- and *MKS3*-silenced cells compared with the negative control. DNA is labelled with DAPI (blue) and the centrosome (γ-tubulin staining) is shown in red. (**D**) Quantification of the presence of a primary cilium in transfected cells. The graph shows mean ± SEM of three independent experiments. At least 1500 cells were counted for each condition. (E–G) As well as the loss of primary cilia seen in control cells (E, arrows), *MKS1*- and *MKS3*-silenced cells have fewer microvilli. (**E'–G'**) Show enlarged 25 $\mu m^2$ regions of the red boxed areas shown in (E–G). Scale bars (C and G) denote 10 μm.

distribution at the cell surface of HEK293 cells, where it co-localizes with a proportion of Myc-MKS1 (arrows in Fig. 8A; top panel). In addition, although endogenous MKS1 was predominantly cytoplasmic, some could also co-localize with wild-type HA-meckelin at the cell surface (arrows in Fig. 4A; third panel). We noted a statistically significant increase (*t*-test: $P < 0.05$) in multinucleated cells over-expressing Myc-MKS1: over 70% of cells transfected and over-expressing Myc-MKS1 after 48 h were multinucleated (Fig. 8A and B), whereas <20% of cells over-expressing MKS3 were multinucleated (Fig. 8B). As MKS1 can localize at the cell surface (Fig. 8A), we evaluated the possibility that MKS1, a soluble protein, can interact with meckelin, a putative receptor. We confirmed a biochemical interaction between meckelin and MKS1 in a series of co-immunoprecipitation experiments (Fig. 8C). These clearly indicated that purified antibodies against meckelin, but not pre-immune serum or antibodies blocked with the cognate peptide, could immunoprecipitate epitope-tagged Myc-MKS1. We also confirmed the reciprocal interaction (immunoprecipitation of epitope-tagged HA-meckelin with anti-MKS1; Fig. 8C).

## DISCUSSION

Many cystic diseases of the kidney have been shown to result from defects in primary cilia, a rapidly expanding area of research. Watnick and Germino (31) originally suggested a unifying pathogenic mechanism for such disorders that, although clinically and pathologically heterogeneous, have a similar outcome. Hildebrandt and Otto (32) reviewed the role of defective primary cilia and basal body proteins in autosomal dominant and recessive polycystic kidney disease (ADPKD1/ADPKD2/ARPKD), nephronophthisis (NPHP), Alström syndrome (ALMS1) and Bardet–Biedl syndrome (BBS). BBS is an autosomal recessive disorder with a phenotypic overlap with MKS. Patients typically present with obesity, retinal degeneration, polydactyly, renal and gonadal malformation and behavioural and developmental problems (33). To date, 12 BBS genes have been identified (*BBS 1–12*). The phenotypes are so similar at the prenatal stage that they may even be indistinguishable and mutations in BBS genes have been found in patients prenatally diagnosed with an MKS-like phenotype: kidney anomalies, polydactyly and brain anomalies, but not encephalocele (34). Recently, PCP signalling has been shown to be disrupted in BBS (35).

Our findings suggest that MKS results from defects in primary cilia and centrosome/basal body function, as expected from the ciliopathy phenotype (36). *In situ* hybridization revealed expression of *MKS3* in the kidneys, liver and digits, which is in keeping with the typical MKS phenotype of cystic kidneys, liver dysplasia and polydactyly. Expression in the retina is consistent with other ciliopathies such as BBS. Retinitis pigmentosa is a common feature of BBS and can result from defective cilia in the rods and cones of the retina. The expression pattern in the brain is especially interesting, with high levels of expression at the midline, in addition to other locations. Defects of the midline, such as agenesis of the corpus callosum and cerebellar vermis, are frequent features of MKS and Joubert syndrome (JBTS). However, it is occipital encephalocele, a defect of the hindbrain, which is considered a diagnostic requirement of MKS. It is significant that *in situ* hybridization detected intense expression of *MKS3* in both the hindbrain (Fig. 1E) and the developing sphenoid bone (Fig. 1F), which forms the base of the skull and joins the basal occipital bone. In contrast, arhinencephaly, a defect of the forebrain is common in MKS, but significant *MKS3* expression was not detected at this location. As *MKS3* expression is also intense in cartilage tissue, it seems more likely that the encephalocele of MKS arises due to

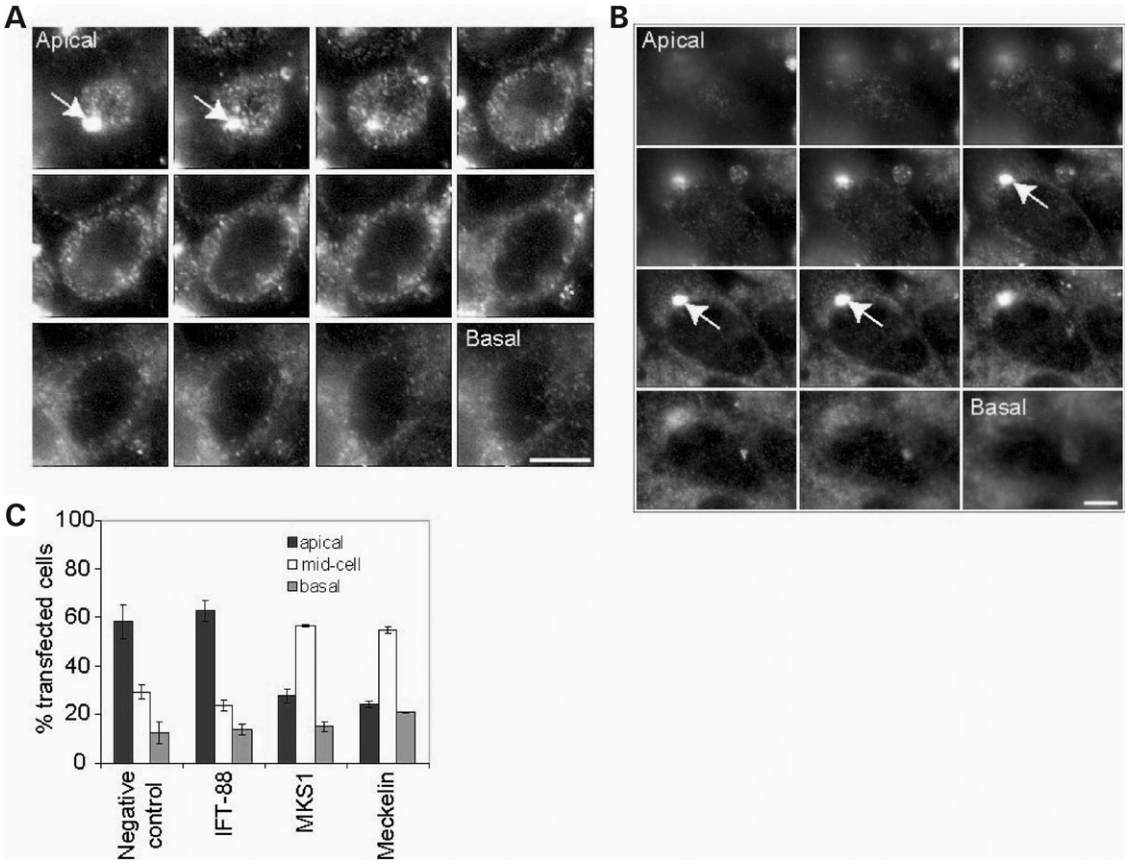


**Figure 6.** Centriole migration fails in *MKS1*- and *MKS3*-silenced cells. Immuofluorescence of IMCD-3 monolayers labelled with γ-tubulin to mark the centrosome, and CM-DiI to label the plasma membrane and internal membranes throughout the cell. Z-stacks were taken and the position of the centrosome assessed. Every second plane of a representative negative control-transfected stack (**A**) and an *MKS3*-silenced stack (**B**) are shown. Note that the centrosome labelling is in the apical region of the cell in control cells (A, arrow), while it is located in the mid-cell region next to the nucleus (visible as a non-stained area) in *MKS3*-silenced cells (B, arrow). *MKS1*-silenced cells gave similar results (see graph, **C**). (C) Quantification of centrosome positioning. Graph represents mean ± SEM of three independent experiments; 500–1000 cells were quantified for each condition. Scale bars (A) and (B) = 5 μm.

defects in the formation of the occipital bone which, unlike the skull vault, develops via a cartilaginous phase (37). Therefore, as suggested previously (38), encephalocele develops as a result of herniation of the meninges and brain through a bony defect, and not from a neural tube closure defect *per se*. Expression of *MKS3* at the midline reiterates the often-noted phenotypic overlap of CNS and other anomalies between MKS and JBTS. Thus, it is probable that these are allelic conditions, with MKS and 'cerebello-oculo-renal syndrome' (39,40) at the severe end of the phenotypic spectrum.

As expected, null alleles for both *MKS3* and *MKS1*, gives rise to a loss of meckelin and MKS1 expression in epithelial cells of the kidney. This is presumably due to nonsense-mediated decay, although we were unable to test this directly because the tissues did not provide useable total RNA. However, a missense mutation (Q376P) in the N-terminal extracellular domain of meckelin (17) results in an inability to localize the mutant protein at the cell surface, predominantly by retention in the ER. Possible mechanisms include the formation of an amino acid sequence that promotes ER retention (41), the occlusion of ER exit codes (42) or aggregation caused by local misfolding.

Our sub-cellular localization studies indicate that MKS1 is located at the centrosomes in dividing cells, and that meckelin can localize at primary cilia. However, meckelin also has a widespread distribution at the cell surface, as demonstrated by both immunofluorescence microscopy and biochemical assays of cell surface processing, and meckelin can interact directly with MKS1. We noted that cells transfected with MKS1 were multinucleated, suggesting that over-expression of this protein may mediate a defect in cell division through a dominant-negative effect and may implicate MKS1 in cell cycle processes. These observations suggest that both proteins have a number of functions, as yet not clearly defined, but with meckelin likely implicated as a membrane receptor involved in signalling events during development.

siRNA-mediated silencing of *MKS1* and *MKS3* revealed that both MKS1 and meckelin play important roles in ciliogenesis. We do not yet know whether there is a direct relationship between cilia and branching in these cells, or if the ciliation defect is a consequence of poor branching. While the topology of meckelin makes it is likely that meckelin mediates signalling events that regulate cilium formation, MKS1 could be a structural protein required for ciliogenesis, or it could be involved in signalling. Elucidation of the binding partners of

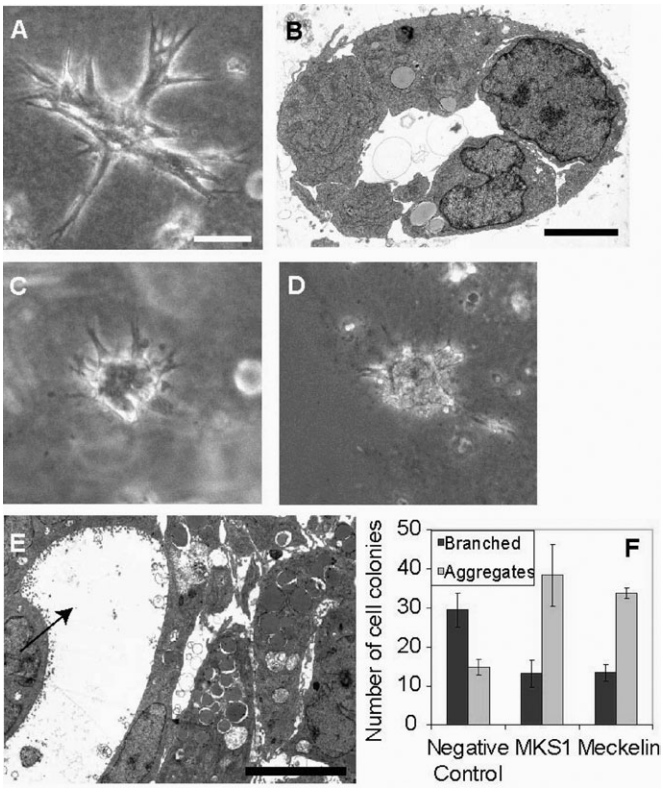


**Figure 7.** MKS1 and meckelin mediate branching morphogenesis during tubulogenesis. Phase contrast (**A, C, D**) and transmission electron microscopy (**B** and **E**) images of IMCD-3 cells cultured for 3 days in three-dimensional collagen I matrix. After 3 days, negative control-transfected cells form highly branched structures (A) and are beginning to form tubule-like structures (B), while *MKS1*- (C) and *MKS3*- (D) silenced cells fail in branching morphogenesis and instead form aggregates of cells containing hollow cysts (E, the arrow indicates the cyst in the mass of cells). (**F**) Quantification of the number of cell colonies forming branched structures and aggregates. Graph shows mean ± SEM of counts from five randomly picked microscope fields. For each condition 150–300 cell colonies were counted. Scale bar (A) =50 μm; (B) =3 μm; (E) = 10 μm.

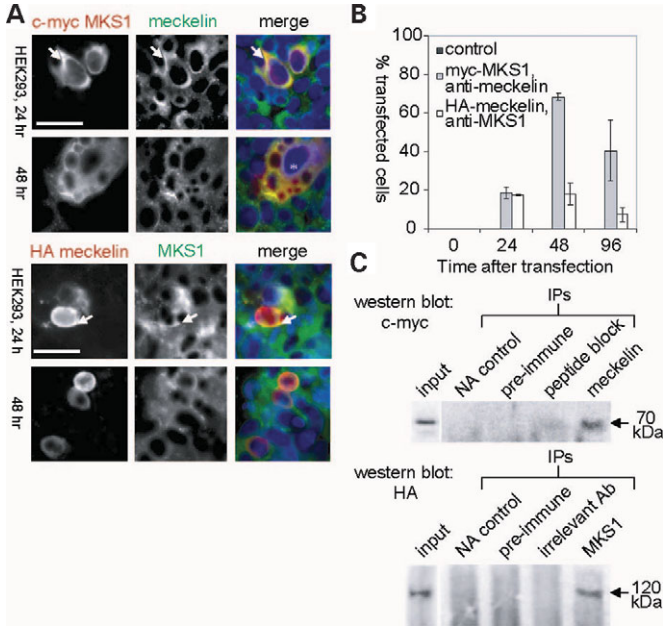


**Figure 8.** MKS1 and meckelin interact. (**A**) Top panels: co-localization of epitope-tagged Myc-MKS1 (left) with endogenous meckelin (centre) at the cell surface, indicated by arrows. A multinucleated cell at 48 h after transfection is indicated by an asterisk. Bottom panels: co-localization of epitope-tagged HA-meckelin (left) with endogenous MKS1 (centre) at the cell surface, indicated by arrows. Full colour merged images are shown on the right. Bar: 10 μm. (**B**) Time-course graph of quantitation of multinucleated cells. Graph shows mean ± SEM of counts from three randomly picked microscope fields. For each condition 200–500 cells were counted. (**C**) Top panel: immunoprecipitation (IP) of epitope-tagged myc-MKS1 from WCEs of transiently transfected HEK293 cells with anti-meckelin (α-meckelin), but not by 'no antibody' (NA control) or pre-immune serum negative controls. IP of endogenous meckelin by anti-meckelin was mostly blocked by treatment of the antiserum with the cognate peptide (peptide block). Bottom panel: IP of epitope-tagged HA-meckelin by anti-MKS1, but not by negative controls or by an irrelevant antibody (anti-V5).

MKS1 and meckelin, and determination of the function of the B9 domain found in MKS1 should help in resolving this issue.

The N-terminal extracellular domain of meckelin is particularly rich in cysteine residues, and is similar to the cysteine-rich domain (CRD) that is found in mammalian orthologues of the *Drosophila frizzled* (*fz*) receptor (43). In *Drosophila*, members of the *frizzled* family of tissue-polarity genes encode cell-surface proteins of the seven transmembrane-domain receptor (7TMR) class, and the CRD in the extracellular region has been implicated as a binding domain for Wnts, cysteine-rich glycoproteins that are homologues of *Drosophila* wingless (19,44). In mammals, the *FZD* family of WNT receptors have a pivotal role in various cellular processes including determination of cell fate, control of cell polarity and malignant transformation (45). Interestingly, PCP signalling has been shown to be disrupted in BBS (35) as well as other ciliopathies. Furthermore, mutations in the human *frizzled-4* gene (*FZD4*) cause an autosomal dominant form of familial exudative vitreoretinopathy (FEVR), which is a hereditary ocular disorder characterized by a failure of peripheral retinal vascularization (20), with loss of visual acuity due to hyperpermeable blood vessels and neovascularization. It remains to be determined if this pathogenic mechanism occurs during renal cytogenesis in MKS.

Centriole movements to the apical membrane are a critical early stage in ciliogenesis. The pathways that control centriole movements during ciliogenesis of the primary cilium are unknown; however, a large body of evidence implicates the actin cytoskeleton in centriole migration in multi-ciliated epithelial cells (46–50) and in the ciliated ctenophore *Beroe* (51). While the signalling events that regulate these processes remain obscure, recent evidence has implicated the PCP effectors inturned (*in*) and fuzzy (*fy*) in the formation of an actin array essential for basal body docking (52). The cytoskeleton is also likely involved in moving the mature centriole during ciliogenesis of the primary cilium, as microtubules position the interphase centrosome (53), while the Rho-associated coiled-coil containing protein kinase p160ROCK is required to maintain the position of the mature centriole in interphase cells (54). Here, we provide the first evidence of factors that control centriole positioning during primary cilium formation. The upstream and downstream pathways which MKS proteins

impinge upon to direct redistribution of the centrioles to the apical membrane remain unknown and require further study, but may involve cell polarity pathways. We speculate that meckelin may act as a non-canonical Wnt receptor that links PCP signalling with actin or tubulin cytoskeleton rearrangments. During *Drosophila* development, the *Drosophila* Rho-associated kinase, Drok, connects frizzled-mediated PCP signalling to the actin cytoskeleton (55), and we suggest that ROCK signalling may be required during ciliogenesis. p160ROCK activity is found at the centrosome (54) and it is possible that MKS1 may provide the link between meckelin at the membrane and ROCK at the centrosome, as it can localize to both regions. Whatever the mechanism, it is likely that MKS1 and meckelin play similar roles in tissues containing primary cilia as well as multi-ciliated epithelia, as both types of tissue can be affected in MKS.

Our results demonstrate a fundamental role for both meckelin and MKS1 in primary cilia and basal body function. MKS therefore joins the increasing list of genetic diseases linked to cilia or basal body dysfunction. Further studies will help to decipher the mechanisms of pathogenicity of MKS, and the role of these proteins in the signalling pathways that mediate development.

## MATERIALS AND METHODS

### Affected individuals and families

All three MKS cases (67F, 40T and 102; see below) had a characteristic MKS phenotype. These comprised the presence of occipital encephalocele, renal cystic dysplasia and evidence of hepatic developmental defects (hepatic fibrosis, bile duct proliferation, ductal plate malformation). Informed consent was obtained from all participating families and the study was approved by the relevant local research Ethics Committees. DNA was extracted from blood, fibroblast cell lines and liver biopsy paraffin blocks using standard methods (56). We performed direct sequencing using the dideoxy chain termination method (ABI 'BigDye 3.0' system) on an ABI 3730 DNA Sequencer, and analysed sequences using Chromas v2.0 software. All mutations were verified bidirectionally.

### Expression vectors

Full-length *MKS1* and *MKS3* ORF clones for FLJ20345 and MGC26979 (IMAGE numbers 3952532 and 4825770) were obtained from Geneservice Ltd., Cambridge, UK for use as templates in PCR. For full-length inserts, amplimers were generated with forward primers that included the start codon, and reverse primers with the native stop codon. For *MKS1*, the forward primer contained an *Eco*RI restriction site (5′-NNNNGAATTCTGGCGGAGACCGTCTGGAGC-3′-), and the reverse primer contained a *Not*I site (5′-NNNNGCGG CCGCCTAGGAGACCAGGGTTCC-3′) for sub-cloning into the pCMV-Myc vector (BD Biosciences Clontech, Palo Alto, CA, USA), giving the pCMV-Myc + MKS1 construct. For *MKS3*, the forward primer contained an *Xho*RI restriction site (5′-NNNNCTCGAGCGGTTTGGTCCCTCTTA-3′-), and the reverse primer contained a *Not*I site (5′-NNNNGCG GCCGCTTAAATCAAAAATCTTTG-3′-) to allow sub-cloning into the pCMV-HA vector (BD Biosciences Clontech), to give the pCMV-HA + MKS3[wt; wild-type] construct. To mimic the effect of the *MKS3* missense mutation c.1127A>C (p.Q376P), we generated a PCR amplimer, using the forward primer as above, and a reverse primer that contained an endogenous *Bgl*II site and a T>G mismatch (5′-ATTAAGATCTTAG AGATAGGAATCTCACAATTT*G*GTTGG-3′), that was sub-cloned into the full-length wild-type insert to give the pCMV-HA + MKS3[mt; Q376P mutant] construct. For *in situ* hybridization studies, a *MKS3* cDNA fragment (nucleotides 2289–3070) was amplified by PCR using the following primers: 5′-TCGACAGTTCGTTGATTTATGC-3′ and 5′-AAAAATATGGCAAACTAACCTGA-3′. The PCR amplimer was sub-cloned into the pGEM-T Easy vector (Promega Ltd., Southampton, UK). All constructs were verified by bidirectional sequencing.

### *In situ* hybridization

Normal human embryos were collected from terminations of pregnancy under the auspices of the Human Developmental Biology Resource (http://www.hdbr.org/) with informed consent of the donors and Ethics Committee approval. *In situ* hybridization was performed on human embryo paraffin sections as described (57). Of a number of *MKS3* cDNA fragments tested as probes for *in situ* hybridization, MKS3 (nucleotides 2289–3070), which contains much of the 3′-UTR of the gene, gave optimal results. Antisense and sense control RNA probes were produced by *in vitro* transcription from the T7 and SP6 RNA polymerase sites, respectively, of pGEM-T Easy vector using the 'Riboprobe' system (Promega). Expression patterns were analysed using the Axioplan 2 imaging system (Zeiss).

### Cells and antibodies

Human renal clear cell (RCC4), human embryonic kidney (HEK293) and mouse inner medullary collecting duct (IMCD-3) cells were grown in Dulbecco's minimal essential medium (DMEM) or in DMEM/Ham's F12 supplemented with 5–10% fetal calf serum (Sigma–Aldrich Co. Ltd., Poole, UK). Biliary epithelial cells (BECs) were isolated and cultured *in vitro* as described previously (58). For functional analyses, IMCD-3 cells were cultured on Transwell permeable supports (#3413, Costar). The following primary antibodies were used: mouse anti-HA and anti-c myc, and rabbit anti-γ-tubulin (all Sigma–Aldrich); mouse anti-β-actin and rabbit anti-calreticulin (Abcam Ltd., Cambridge, UK); goat anti-EEA1 (Santa Cruz Technology, CA, USA); mouse anti E-cadherin (BD Transduction Laboratories), rat anti-ZO-1 (Zymed) and anti-acetylated alpha tubulin clone C3B9 (59). Secondary antibodies were: fluorescein isothiocyanate (FITC)-, tetramethyl rhodamine isothiocyanate (TRITC)- and horseradish peroxidase (HRP)-conjugated goat anti-mouse and anti-rabbit immunoglobulins, and rabbit anti-goat conjugates (Sigma–Aldrich), Alexa-fluor 488- and Alexa-fluor 594-conjugated goat anti-mouse and goat anti-rabbit (Molecular Probes) and rhodamine-conjugated goat anti-rat (Jackson Immunoresearch). CM-DiI was from Molecular Probes.

### Polyclonal antibody production

Polyclonal antisera to MKS1 and meckelin were raised in rabbits by immunization with synthetic peptides: ETEGEKQELWKYTI-(C) and (C)-NLASKTLVDQRFLI, which correspond to internal sequence in MKS1 (residues 109–122) and the C-terminus of meckelin (residues 982–995). Cysteine residues (C) were included to enable covalent cross-linking. Antisera were raised commercially (Sigma–Aldrich Corp. and CovalAb UK Ltd., Cambridge, UK) and were characterized by ELISA and western blotting using standard methodologies (60). For co-immunoprecipitation experiments, we purified small volumes (2 ml) of antisera by passing them through a column containing protein A-sepharose beads (GE Healthcare UK Ltd., Little Chalfont, UK), essentially as described previously (61).

### Whole cell extract preparation and western blotting

Whole cell extracts (WCEs) were prepared from HEK293 or IMCD-3 cells. Approximately, $5 \times 10^7$ cells were scraped into PBS, washed and resuspended in lysis buffer [50 mM Tris, pH 7.5, 150 mM NaCl, 0.5 mM EDTA, 0.5 mM EGTA, 0.02% (w/v) $NaN_3$, 1.0% (v/v) Igepal C630 (Sigma–Aldrich), 10% (v/v) glycerol, 0.1% (v/v) protease inhibitor cocktail for mammalian cell extracts in DMSO, Sigma–Aldrich]. The cell suspension was incubated on ice for 30 min with gentle stirring, sonicated on ice and clarified by centrifuging at 13 000*g* for 5 min. WCE was also prepared from transiently transfected cells for use in co-immunoprecipitation experiments (see below).

For western blotting, 10 μg WCE total protein was analysed by 8% SDS–PAGE and transferred to activated 'Invitrolon' PVDF membrane (Invitrogen) using 1× CAPS transfer buffer, pH 11 (56). Proteins were immunodetected by standard methods (60). Rabbit polyclonal antisera or mouse monoclonal antibodies (MAbs) were used at final dilutions of 200× to 1000× for polyclonals and 1000× to 5000× for MAbs. Appropriate HRP-conjugated secondary antibodies (Sigma–Aldrich) were used (at 5000× to 10 000× dilutions) for detection by the enhanced chemiluminescence (ECL) plus western blotting detection system (GE Healthcare UK Ltd., Little Chalfont, UK).

### Immunohistochemistry

Human fetal (weeks 18–20) tissues for immunohistochemical detection of MKS1 and meckelin were obtained at autopsy from either three MKS cases or two gestationally age-matched controls that had undergone therapeutic termination for intrauterine infection. *MKS3* mutations have been described previously (17) in two of the MKS cases in the present study: 67F with frameshift mutation c.647delA (p.E216fsX221) and 40T the missense mutation c.1127A>C (p.Q376P). The third case, 102, with typical features of MKS, has a novel *MKS1* c.1448_1451dupCAGG duplication causing a frameshift mutation (p.T485fsX591). Tissues were fixed in 10% formaldehyde and embedded in paraffin. Thin sections (4 μm) of liver and kidney tissues were cut onto slides, deparaffinized in two 5 min incubations of clean xylene and rehydrated by a 100, 95, 70 and 50% ethanol series. Epitope recovery was through boiling in 1 mM EDTA pH 8.0, by microwaving at reduced power, for 15 min followed by 30 min cooling. Endogenous peroxidase activity was inactivated by incubation in 3% $H_2O_2$/50% methanol for 30 min, followed by washing in TBST [50 mM Tris, pH 7.5, 135 mM NaCl, 2.7 mM KCl, 0.05% (v/v) Tween 20]. Sections were blocked in diluent buffer supplemented with 5% normal goat serum for 1 h at room temperature. Primary antibodies (rabbit polyclonal antisera at 250× to 500× dilutions in diluent buffer, matched to appropriate pre-immune negative control sera) were applied to the slides in a moist chamber for 18 h at 4°C. Slides were washed thoroughly with TBST, and the secondary antibody (goat anti-rabbit HRP-IgG conjugate; Sigma–Aldrich) was applied at a dilution of 250×. Sections were developed in 'Sigma Fast' 3,3′-diaminobenzidine (DAB) with $CoCl_2$ enhancer and counterstained with Meyer's hematoxylin (Sigma–Aldrich). Sections were dehydrated in an ethanol series, cleared in xylene and mounted with 'CV Mount' (Leica Instruments GmbH, Nussloch, Germany).

### Transient transfection

For transient transfection experiments, cells were grown on glass coverslips (22 mm × 22 mm, placed in a six-well plate) to ~80% confluence, transfected with 0.4 μg of plasmid DNA (pCMV-HA or pCMV-Myc empty vector, pCMV-HA + MKS3[wt], pCMV-HA + MKS3[mt] or pCMV-Myc + MKS1 constructs) using 'Effectene' reagent (Qiagen GmbH, Hilden, Germany) for 24 h. Transfection complexes were removed and cells were allowed to grow for a further 24 h in normal medium prior to fixation.

### siRNA of MKS1 and MKS3

siRNA duplexes were designed against different regions of the *Mks1* or *Mks3* sequence using Dharmacon's custom SMARTpool siRNA service (mouse Tmem67; NCBI accession no. NM_177861): 5′-UAAAUCGGAAAAUCUCUUGUU-3′, 5′-AAAUACGUUCUCCAUAUGCUU-3′, 5′-UUUCUCGCCCACUUACUGCUU-3′, 5′-CAAUCUGAAACGUCUGCCCUU-3′ or Invitrogen's Stealth siRNA service (mouse *Mks1*; NCBI accession no. AK190930): 5′-AUUCUUUGCAGAUGAACUCGGAGGC-3′, 5′-GCCUCCGAGUUCAUCUGCAAAGAAU-3′, 5′-GUCAGUGUAAGUGAAGAUUCGCCGG-3′. The medium GC non-targeting negative control (Invitrogen) was used as a negative control, and SMARTpool siRNA against IFT-88 (mouse Tg737; NCBI accession no. NP_033402, Dharmacon) was used as a positive control for loss of cilia. siRNA was pooled and 100 pmol of each siRNA was simultaneously transfected into IMCD-3 cells at 50–70% confluency using Lipofectamine 2000 (Invitrogen) according to the manufacturer's instructions. Transfected cells were identified using a fluorescent oligo transfection marker (Invitrogen). Assays were carried out at 96 h after transfection. Quantitative real-time PCR was used to measure the decrease of *Mks1* or *Mks3* transcript levels following siRNA treatment, essentially as described previously (17). Two sets of independent assays were each run in triplicate. PCR analysis of cDNA was performed using denaturing HPLC-purified primers specific that spanned at least one

exon–intron boundary for *Mks1* (exons 6–7: forward 5′-GAGGGCAGCAAACTCAAGTC-3′ and reverse 5′-TTC ACTGTGATCACGCCATT-3′), *Mks3* (exons 22–24: forward 5′- GTTTGTTGACCTGTGCTCCA-3′ and reverse 5′-ATCTGAAACGTCTGCCCATC-3′) and *Hprt* as a normalizing control (exons 1–3: forward 5′-CCAGCGTCGTGA TTAGCGATG-3′ and reverse 5′-ATAGCCCCCCTTGAGCA CACAGAG-3′).

### Immuofluorescence microscopy

For transient transfection experiments and localization of MKS1 and meckelin, cells were fixed in 4% paraformaldehyde in PBS for 30 min and blocked in PBST buffer [1× PBS, 0.1% (v/v) Tween 20] supplemented with 5% (v/v) normal goat serum. Epitope-tagged and/or endogenous proteins were detected by application of antibodies diluted 100× in diluent buffer. Primary antibodies were detected by application of FITC- and/or TRITC-conjugated goat anti-rabbit or anti-mouse IgG antibodies diluted 250× in diluent buffer. For immunolocalization studies on siRNA cells, cells were extracted in 0.75% Triton X-100 in 100 mM PIPES, pH 6.9, 2 mM EGTA, 1 mM $MgSO_4$, 0.1 mM EDTA for 30 s and fixed in methanol at −20°C for at least 10 min. Samples were rehydrated in PBS for 10 min prior to incubation with primary and secondary antibodies. Anti-fade (Vectashield, Vector Laboratories Ltd., Peterborough, UK) containing DAPI was applied, and samples were examined with a Zeiss Axioplan or Axioplan 2 epifluorescence microscope equipped with a motorized stage and using a 100×, 1.4NA oil immersion lens. Images were captured on a CCD camera controlled by either SmartCapture 2 software (Digital Scientific Ltd., Cambridge, UK) or Metamorph software (Universal Imaging), and processed in Metamorph and Adobe Photoshop (Adobe).

### Immunoprecipitation of immunocomplexes

WCEs were prepared from HEK293 cells that had been transiently transfected with 2.0 μg of plasmid DNA [empty vectors as controls, and the pCMV-HA + MKS3(wt), pCMV-HA + MKS3(mt) or pCMV-Myc + MKS1 constructs] in 90 mM tissue culture dishes. WCE supernatants were processed for immunoprecipitation experiments using 5 μg purified anti-HA or anti-c-myc MAb, or 5 μg purified IgG fractions from rabbit polyclonal antisera, coupled to protein G- and/or protein A-sepharose beads (GE Healthcare UK Ltd.) essentially as described previously (61).

### Biotinylation of cell surface proteins

Transiently transfected HEK293 cells in 90 mm dishes were grown to confluence, washed thoroughly with ice-cold 1× PBS and incubated with 0.5 mg/ml sulfo-NHS-SS-biotin (Perbio Science UK Ltd., Cramlington, UK) for 30 min at 4°C. The reaction was quenched with 50 mM ammonium chloride. Cells were lysed and WCEs prepared as described above. Biotinylated cell surface proteins were recovered by binding to streptavidin-agarose beads (Sigma–Aldrich) for 2 h at 4°C. After washing, the beads were resuspended in SDS–PAGE loading buffer (containing fresh 2-mercaptoethanol), incubated at 37°C for 20 min and loaded on to 8% SDS–PAGE gels. Epitope-tagged meckelin was immunodetected by western blotting.

### Measurement of transepithelial resistance

IMCD-3 cells were grown and transfected as above and cultured on Transwell filters for a further 4 days. Transepithelial resistance measurements were made using a Millicell-ERS meter (Millipore).

### Electron microscopy

IMCD-3 cells were grown on 13 mm glass coverslips, transfected as above and cultured for a further 4 days. Cells for transmission electron microscopy were fixed by addition of 2.5% gluteraldehyde, 2% paraformaldehyde and 0.1% picric acid in 100 mM phosphate (pH 6.5) to the culture medium followed by post-fixation in 1% osmium tetraoxide in 100 mM phosphate buffer (pH 6.5) for 1 h at 4°C. The fixed material was stained *en bloc* with 2% aqueous uranyl acetate for 2 h at 4°C. Following dehydration through a graded series of acetone and propylene oxide, the material was embedded in epon resin for sectioning. Samples fixed as above were prepared for scanning electron microscopy essentially as described (62).

### Culture of IMCD-3 cells in type I collagen gels

IMCD-3 cells were cultured in three-dimensional collagen gels as previously described (63). To assess branching morphogenesis in MKS1- or meckelin-depleted cells, IMCD-3 cells were grown on 30 mm tissue culture dishes (Falcon) to 30–50% confluency, transfected with appropriate siRNAs as above and left for 24 h before trypsinization and plating into collagen in 96-well tissue culture plates. Two hundred microlitres of tissue culture medium containing 10% fetal calf serum was added to the top of each solidified gel. After 72 h, gels were fixed in 2.5% gluteraldehyde, 2% paraformaldehyde and 0.1% picric acid in 100 mM phosphate (pH 6.5) for 2 h at room temperature, examined using 10× phase contrast optics on a Zeiss Axioskop microscope and captured on a CCD camera controlled by IPLab software (Scanalytics Inc., BD Biosciences).

## ACKNOWLEDGEMENTS

We would like to thank Mike Shaw (University of Oxford) for assistance with E.M., and the Queen Elizabeth University Hospital Liver and Hepatobiliary Surgical Unit in procurement of liver tissue. We thank Dr Esther Maina for advice on quantitative real-time PCR and Dr Paloma Garcia for the gift of mouse *Hprt* primers. Work in our laboratories was funded by the BBSRC, the Wellcome Trust, University of Birmingham Medical School 'Scientific Projects', Children's Liver Disease Foundation, Birmingham Children's Hospital Research Foundation, Birmingham Women's Hospital R&D Fund and the E.P. Abraham Trust. J.L.B. is supported by a grant from the Polycystic Kidney Disease Foundation. The Human Developmental Biology Resource (D.G. and A.J.C.)

is supported by the MRC and Wellcome Trust. H.R.D. is a Beit Memorial Research Fellow; K.G. is a Wellcome Trust Principal Research Fellow.

*Conflict of Interest statement*. None declared.

## REFERENCES


1. Meckel, J.F. (1822) Beschreibung zweier, durch sehr aehnliche Bildungsabweichungen entstellter Geschwister. *Dtsch. Arch. Physiol.*, **7**, 99–172.
2. Gruber, G.B. (1934) Beitraege zur Frage 'gekoppelter'Missbildungen. (Akrocephalo-Syndactylie und Dysencephalia splanchnocystica). *Beitr. Path. Anat.*, **93**, 459–476.
3. Opitz, J.M. and Howe, J.J. (1969) The Meckel syndrome (dysencephalia splanchnocystica, the Gruber syndrome). *Birth Defects Orig. Art. Ser.*, **V**, 167–179.
4. Salonen, R. (1984) The Meckel syndrome: clinicopathological findings in 67 patients. *Am. J. Med. Genet.*, **18**, 671–689.
5. Salonen, R. and Paavola, P. (1998) Meckel syndrome. *J. Med. Genet.*, **35**, 497–501.
6. Mecke, S. and Passarge, E. (1971) Encephalocele, polycystic kidneys, and polydactyly as an autosomal recessive trait simulating certain other disorders: the Meckel syndrome. *Ann. Genet.*, **14**, 97–103.
7. Fraser, F.C. and Lytwyn, A. (1981) Spectrum of anomalies in the Meckel syndrome, or: 'Maybe there is a malformation syndrome with at least one constant anomaly'. *Am. J. Med. Genet.*, **9**, 67–73.
8. Ahdab-Barmada, M. and Claassen, D. (1990) A distinctive triad of malformations of the central nervous system in the Meckel–Gruber syndrome. *J. Neuropathol. Exp. Neurol.*, **49**, 610–620.
9. Holmes, L.B., Driscoll, S.G. and Atkins, L. (1976) Etiologic heterogeneity of neural-tube defects. *N. Engl. J. Med.*, **294**, 365–369.
10. Paavola, P., Salonen, R., Weissenbach, J. and Peltonen, L. (1995) The locus for Meckel syndrome with multiple congenital anomalies maps to chromosome 17q21-q24. *Nat. Genet.*, **11**, 213–215.
11. Kyttälä, M., Tallila, J., Salonen, R., Kopra, O., Kohlschmidt, N., Paavola-Sakki, P., Peltonen, L. and Kestila, M. (2006) MKS1, encoding a component of the flagellar apparatus basal body proteome, is mutated in Meckel syndrome. *Nat. Genet.*, **38**, 155–157.
12. Gherman, A., Davis, E.E. and Katsanis, N. (2006) The ciliary proteome database: an integrated community resource for the genetic and functional dissection of cilia. *Nat. Genet.*, **38**, 961–962.
13. Badano, J.L., Mitsuma, N., Beales, P.L. and Katsanis, N. (2006) The ciliopathies: an emerging class of human genetic disorders. *Annu. Rev. Genom. Hum. Genet.*, **7**, 125–148.
14. Roume, J., Ma, H.W., Le Merrer, M., Cormier-Daire, V., Girlich, D., Genin, E. and Munnich, A. (1997) Genetic heterogeneity of Meckel syndrome. *J. Med. Genet.*, **34**, 1003–1006.
15. Roume, J., Genin, E., Cormier-Daire, V., Ma, H.W., Mehaye, B., Attie, T., Razavi-Encha, F., Fallet-Bianco, C., Buenerd, A., Clerget-Darpoux, F. *et al*. (1998) A gene for Meckel syndrome maps to chromosome 11q13. *Am. J. Hum. Genet.*, **63**, 1095–1101.
16. Morgan, N.V., Gissen, P., Sharif, S.M., Baumber, L., Sutherland, J., Kelly, D.A., Aminu, K., Bennett, C.P., Woods, C.G., Mueller, R.F. *et al*. (2002) A novel locus for Meckel–Gruber syndrome, MKS3, maps to chromosome 8q24. *Hum. Genet.*, **111**, 456–461.
17. Smith, U.M., Consugar, M., Tee, L.J., McKee, B.M., Maina, E.N., Whelan, S., Morgan, N.V., Goranson, E., Gissen, P., Lilliquist, S. *et al*. (2006) The transmembrane protein meckelin (MKS3) is mutated in Meckel–Gruber syndrome and the wpk rat. *Nat. Genet.*, **38**, 191–196.
18. Gattone, V.H., II., Tourkow, B.A., Trambaugh, C.M., Yu, A.C., Whelan, S., Phillips, C.L., Harris, P.C. and Peterson, R.G. (2004) Development of multi-organ pathology in the wpk rat model of polycystic kidney disease. *Anat. Rec. A. Discov. Mol. Cell. Evol. Biol.*, **277**, 384–395.
19. Moon, R.T., Kohn, A.D., De Ferrari, G.V. and Kaykas, A. (2004) WNT and beta-catenin signalling: diseases and therapies. *Nat. Rev. Genet.*, **5**, 691–701.
20. Robitaille, J., MacDonald, M.L., Kaykas, A., Sheldahl, L.C., Zeisler, J., Dube, M.P., Zhang, L.H., Singaraja, R.R., Guernsey, D.L., Zheng, B. *et al*. (2002) Mutant frizzled-4 disrupts retinal angiogenesis in familial exudative vitreoretinopathy. *Nat. Genet.*, **32**, 326–330.
21. Strutt, D. (2003) Frizzled signalling and cell polarisation in *Drosophila* and vertebrates. *Development*, **130**, 4501–4513.
22. Efimenko, E., Bubb, K., Mak, H.Y., Holzman, T., Leroux, M.R., Ruvkun, G., Thomas, J.H. and Swoboda, P. (2005) Analysis of *xbx* genes in *C. elegans*. *Development*, **132**, 1923–1934.
23. Melton, D.W. (1981) Cell fusion-induced mouse neuroblastomas HPRT revertants with variant enzyme and elevated HPRT protein levels. *Somatic Cell. Genet.*, **7**, 331–344.
24. Pazour, G.J., Dickert, B.L., Vucica, Y., Seeley, E.S., Rosenbaum, J.L., Witman, G.B. and Cole, D.G. (2000) Chlamydomonas IFT88 and its mouse homologue, polycystic kidney disease gene *tg737*, are required for assembly of cilia and flagella. *J. Cell Biol.*, **151**, 709–718.
25. Matter, K. and Balda, M.S. (2003) Functional analysis of tight junctions. *Methods*, **30**, 228–234.
26. Zegers, M.M., O'Brien, L.E., Yu, W., Datta, A. and Mostov, K.E. (2003) Epithelial polarity and tubulogenesis *in vitro*. *Trends Cell Biol.*, **13**, 169–176.
27. Henneguy, L.F. (1898) Sur les rapports des cils vibratiles avec les centrosomes. *Archives d'Anatomie Microscopique*, **Tome 1**, 481–496.
28. Lenhossek, M. (1898) Ueber Flimmerzellen. *Verhandl. der Anat. Gesel*, **12**, 106–128.
29. Cantley, L.G., Barros, E.J., Gandhi, M., Rauchman, M. and Nigam, S.K. (1994) Regulation of mitogenesis, motogenesis, and tubulogenesis by hepatocyte growth factor in renal collecting duct cells. *Am. J. Physiol.*, **267**, F271–F280.
30. Piscione, T.D., Yager, T.D., Gupta, I.R., Grinfeld, B., Pei, Y., Attisano, L., Wrana, J.L. and Rosenblum, N.D. (1997) BMP-2 and OP-1 exert direct and opposite effects on renal branching morphogenesis. *Am. J. Physiol.*, **273**, F961–F975.
31. Watnick, T. and Germino, G. (2003) From cilia to cyst. *Nat. Genet.*, **34**, 355–356.
32. Hildebrandt, F. and Otto, E. (2005) Cilia and centrosomes: a unifying pathogenic concept for cystic kidney disease? *Nat. Rev. Genet.*, **6**, 928–940.
33. Katsanis, N. (2004) The oligogenic properties of Bardet–Biedl syndrome. *Hum. Mol. Genet.*, **13** (Spec no. 1), R65–R71.
34. Karmous-Benailly, H., Martinovic, J., Gubler, M.C., Sirot, Y., Clech, L., Ozilou, C., Auge, J., Brahimi, N., Etchevers, H., Detrait, E. *et al*. (2005) Antenatal presentation of Bardet–Biedl syndrome may mimic Meckel syndrome. *Am. J. Hum. Genet.*, **76**, 493–504.
35. Ross, A.J., May-Simera, H., Eichers, E.R., Kai, M., Hill, J., Jagger, D.J., Leitch, C.C., Chapple, J.P., Munro, P.M., Fisher, S. *et al*. (2005) Disruption of Bardet–Biedl syndrome ciliary proteins perturbs planar cell polarity in vertebrates. *Nat. Genet.*, **37**, 1135–1140.
36. Badano, J.L., Teslovich, T.M. and Katsanis, N. (2005) The centrosome in human genetic disease. *Nat. Rev. Genet.*, **6**, 194–205.
37. Hanken, J. and Thorogood, P. (1993) Evolution and development of the vertebrate skull: the role of pattern formation. *Trends Ecol. Evol.*, **8**, 9–14.
38. Harding, B.N. and Copp, A.J. (2002) *Congenital Malformations*, Arnold, London.
39. Keeler, L.C., Marsh, S.E., Leeflang, E.P., Woods, C.G., Sztriha, L., Al-Gazali, L., Gururaj, A. and Gleeson, J.G. (2003) Linkage analysis in families with Joubert syndrome plus oculo-renal involvement identifies the CORS2 locus on chromosome 11p12-q13.3. *Am. J. Hum. Genet.*, **73**, 656–662.
40. Valente, E.M., Salpietro, D.C., Brancati, F., Bertini, E., Galluccio, T., Tortorella, G., Briuglia, S. and Dallapiccola, B. (2003) Description, nomenclature, and mapping of a novel cerebello-renal syndrome with the molar tooth malformation. *Am. J. Hum. Genet.*, **73**, 663–670.
41. Chang, X.B., Cui, L., Hou, Y.X., Jensen, T.J., Aleksandrov, A.A., Mengos, A. and Riordan, J.R. (1999) Removal of multiple arginine-framed trafficking signals overcomes misprocessing of delta F508 CFTR present in most patients with cystic fibrosis. *Mol. Cell.*, **4**, 137–142.
42. Nishimura, N. and Balch, W.E. (1997) A di-acidic signal required for selective export from the endoplasmic reticulum. *Science*, **277**, 556–558.
43. Xu, Y.K. and Nusse, R. (1998) The frizzled CRD domain is conserved in diverse proteins including several receptor tyrosine kinases. *Curr. Biol.*, **8**, R405–R406.
44. Bhanot, P., Brink, M., Samos, C.H., Hsieh, J.C., Wang, Y., Macke, J.P., Andrew, D., Nathans, J. and Nusse, R. (1996) A new member of the

frizzled family from *Drosophila* functions as a Wingless receptor. *Nature*, **382**, 225–230.
45. Cadigan, K.M. and Nusse, R. (1997) Wnt signaling: a common theme in animal development. *Genes Dev.*, **11**, 3286–3305.
46. Boisvieux-Ulrich, E., Laine, M.C. and Sandoz, D. (1987) *In vitro* effects of benzodiazepines on ciliogenesis in the quail oviduct. *Cell Motil. Cytos.*, **8**, 333–344.
47. Boisvieux-Ulrich, E., Laine, M. and Sandoz, D. (1990) Cytochalasin D inhibits basal body migration and ciliary elongation in quail oviduct epithelium. *Cell Tissue Res.*, **259**, 443–454.
48. Klotz, C., Bordes, N., Laine, M.C., Sandoz, D. and Bornens, M. (1986) Myosin at the apical pole of ciliated epithelial cells as revealed by a monoclonal antibody. *J. Cell Biol.*, **103**, 613–619.
49. Lemullois, M., Boisvieux-Ulrich, E., Laine, M.C., Chailley, B. and Sandoz, D. (1988) Development and functions of the cytoskeleton during ciliogenesis in metazoa. *Biol. Cell*, **63**, 195–208.
50. Lemullois, M., Klotz, C. and Sandoz, D. (1987) Immunocytochemical localization of myosin during ciliogenesis of quail oviduct. *Eur. J. Cell Biol.*, **43**, 429–437.
51. Tamm, S. and Tamm, S.L. (1988) Development of macrociliary cells in Beroe. I. Actin bundles and centriole migration. *J. Cell Sci.*, **89**, 67–80.
52. Park, T.J., Haigo, S.L. and Wallingford, J.B. (2006) Ciliogenesis defects in embryos lacking inturned or fuzzy function are associated with failure of planar cell polarity and Hedgehog signaling. *Nat. Genet.*, **38**, 303–311.
53. Burakov, A., Nadezhdina, E., Slepchenko, B. and Rodionov, V. (2003) Centrosome positioning in interphase cells. *J. Cell Biol.*, **162**, 963–969.
54. Chevrier, V., Piel, M., Collomb, N., Saoudi, Y., Frank, R., Paintrand, M., Narumiya, S., Bornens, M. and Job, D. (2002) The Rho-associated protein kinase p160ROCK is required for centrosome positioning. *J. Cell Biol.*, **157**, 807–817.
55. Winter, C.G., Wang, B., Ballew, A., Royou, A., Karess, R., Axelrod, J.D. and Luo, L. (2001) *Drosophila* Rho-associated kinase (Drok) links frizzled-mediated planar cell polarity signaling to the actin cytoskeleton. *Cell*, **105**, 81–91.
56. Sambrook, J. and Russell, D. (2000) *Molecular Cloning: A Laboratory Manual*, Cold Spring Harbor Laboratory Press, NY, USA.
57. Lai, C.S., Gerrelli, D., Monaco, A.P., Fisher, S.E. and Copp, A.J. (2003) FOXP2 expression during brain development coincides with adult sites of pathology in a severe speech and language disorder. *Brain*, **126**, 2455–2462.
58. Afford, S.C., Ahmed-Choudhury, J., Randhawa, S., Russell, C., Youster, J., Crosby, H.A., Eliopoulos, A., Hubscher, S.G., Young, L.S. and Adams, D.H. (2001) CD40 activation-induced, Fas-dependent apoptosis and NF-kappaB/AP-1 signaling in human intrahepatic biliary epithelial cells. *FASEB J.*, **15**, 2345–2354.
59. Woods, A., Sherwin, T., Sasse, R., MacRae, T.H., Baines, A.J. and Gull, K. (1989) Definition of individual components within the cytoskeleton of *Trypanosoma brucei* by a library of monoclonal antibodies. *J. Cell Sci.*, **93**, 491–500.
60. Harlow, E. and Lane, D. (1998) *Using Antibodies: A Laboratory Manual*, Cold Spring Harbor Laboratory Press, NY, USA.
61. Johnson, C.A., Padget, K., Austin, C.A. and Turner, B.M. (2001) Deacetylase activity associates with topoisomerase II and is necessary for etoposide-induced apoptosis. *J. Biol. Chem.*, **276**, 4539–4542.
62. Sherwin, T. and Gull, K. (1989) The cell division cycle of *Trypanosoma brucei brucei*: timing of event markers and cytoskeletal modulations. *Phil. Trans. R. Soc. Lond. B Biol. Sci.*, **323**, 573–588.
63. Leung-Hagesteijn, C., Hu, M.C., Mahendra, A.S., Hartwig, S., Klamut, H.J., Rosenblum, N.D. and Hannigan, G.E. (2005) Integrin-linked kinase mediates bone morphogenetic protein 7-dependent renal epithelial cell morphogenesis. *Mol. Cell. Biol.*, **25**, 3648–3657.